

The Stochastic Finite Element Method: Theory and Applications

George Stefanou

Institute of Structural Analysis and Seismic Research
National Technical University of Athens, Greece

Clermont-Ferrand
June 2009

4/6/2009

IFMA Seminar, France

1

Outline of the presentation

- Stochastic processes and fields
- Simulation of Gaussian stochastic processes/fields
- Simulation of non-Gaussian stochastic processes/fields
- The stochastic finite element method (SFEM)
- SFE (static) analysis of shells with random material and geometric properties - response variability calculation
- SFE-based stability analysis of shells with random imperfections
- Nonlinear dynamic analysis of frames with random material properties under seismic loading

4/6/2009

IFMA Seminar, France

2

Simulation of Gaussian stochastic fields

➤ The spectral representation method (Rice 1954, Shinozuka & Deodatis 1991)

Fundamental theorem:
$$f(x) = \int_0^{\infty} [\cos(\kappa x) du(\kappa) + \sin(\kappa x) dv(\kappa)] \longrightarrow$$

Spectral representation of field $f(x)$:
$$\hat{f}(x) = \sum_{n=0}^{N-1} A_n \cos(\kappa_n x + \Phi_n)$$

$$A_n = \sqrt{2S_{ff}(\kappa_n)\Delta\kappa}$$

$$\kappa_n = n\Delta\kappa$$

$$\Delta\kappa = \frac{\kappa_u}{N}$$

Truncated form (finite number of terms)

$$n = 0, 1, 2, \dots, N-1$$

✓ $\hat{f}(x)$ is asymptotically a Gaussian stochastic field as $N \rightarrow \infty$ due to the central limit theorem

✓ Its mean value and autocorrelation function are identical to the corresponding targets as $N \rightarrow \infty$

✓ $\hat{f}(x)$ is periodic with period T_0 :
$$T_0 = \frac{2\pi}{\Delta\kappa}$$

The Fast Fourier Transform (FFT):
$$\hat{f}^{(i)}(p\Delta x) = \text{Re} \left[\sum_{n=0}^{M-1} B_n e^{i \left(\frac{np2\pi}{M} \right)} \right]$$

$$B_n = \sqrt{2} A_n e^{i\phi_n^{(i)}}$$

$$n = 0, 1, \dots, M-1$$

$$p = 0, 1, \dots, M-1$$

M is the number of points on which f is generated: $M = 2^{\mu}$

✓ FFT-based sample functions are always generated on a domain equal to one period T_0

✓ The reduction of step Δx (stochastic mesh refinement) leads to a larger number of terms M in the FFT series

➤ The Karhunen-Loève expansion method (Loève 1977, Ghanem & Spanos 1991)

$$f(x, \theta) = \mu(x) + \sum_{n=1}^{\infty} \sqrt{\lambda_n} \phi_n(x) \xi_n(\theta) \longrightarrow \hat{f}(x, \theta) = \mu(x) + \sum_{n=1}^N \sqrt{\lambda_n} \phi_n(x) \xi_n(\theta)$$

Exact form (infinite terms) Truncated form (finite number of terms)

$\lambda_n, \phi_n(x)$ eigenpairs of the covariance function $C_{ff}(x_1, x_2)$ obtained from the solution of the following eigenvalue problem:

$$\int_D C_{ff}(x_1, x_2) \phi_n(x_1) dx_1 = \lambda_n \phi_n(x_2) \quad (\text{Fredholm integral equation of the second kind})$$

- ✓ Exact solution feasible only for simple geometries and special forms of $C_{ff}(x_1, x_2)$
- ✓ Numerical solution with the conventional Galerkin approach → Dense matrices very costly to compute and invert

• Some remarks on K-L expansion

- ✓ Few K-L terms are needed for the simulation of strongly correlated (narrow-banded) stochastic fields
- ✓ Few K-L terms are needed for the simulation of stochastic fields with smooth (differentiable) target covariance function
- ✓ More efficient simulation when the exact (analytical) solution of the eigenvalue problem is feasible (Huang et al. 2001)
- ✓ The variance of the stochastic field is underestimated and the simulated field $\hat{f}(x, \theta)$ is in general **not** homogeneous since its variance is a function of x (Field & Grigoriu 2004):

$$Var[\hat{f}(x, \theta)] = \sum_{n=1}^N [\sqrt{\lambda_n} \phi_n(x)]^2 \leq \sum_{n=1}^{\infty} [\sqrt{\lambda_n} \phi_n(x)]^2 = Var[f(x, \theta)]$$

• Non-ergodic characteristics of K-L sample functions (Stefanou & Papadarakis 2007)

- Ergodicity in the mean: $\Pr \left\{ \lim_{L \rightarrow \infty} \langle f(x) \rangle_L = E[f(x)] \right\} = 1$

Proof:

Without any loss of generality, we consider that $E[f(x)] = \bar{f}(x) = 0$

$$\langle \hat{f}^{(i)}(x) \rangle_L = \frac{1}{L} \int_0^L \hat{f}^{(i)}(x) dx = \frac{1}{L} \int_0^L \sum_{n=1}^N \sqrt{\lambda_n} \xi_n^{(i)} \phi_n(x) dx = \frac{1}{L} \sum_{n=1}^N \sqrt{\lambda_n} \xi_n^{(i)} \int_0^L \phi_n(x) dx$$

$$\begin{aligned} \lim_{L \rightarrow \infty} \langle \hat{f}^{(i)}(x) \rangle_L &= \lim_{L \rightarrow \infty} \left[\frac{1}{L} \sum_{n=1}^N \sqrt{\lambda_n} \xi_n^{(i)} \int_0^L \phi_n(x) dx \right] \\ &= \sum_{n=1}^N \sqrt{\lambda_n} \xi_n^{(i)} \underbrace{\lim_{L \rightarrow \infty} \left[\frac{1}{L} \int_0^L \phi_n(x) dx \right]}_{=?} \end{aligned}$$

- ✓ Existence of limit
- ✓ Right hand side of the expression: random variable
- ✓ K-L sample functions: in general not ergodic in the mean

- Ergodicity in autocorrelation: $\hat{R}_{ff}^{(i)}(\xi) = R_{ff}^T(\xi) \quad \forall \hat{f}^{(i)}(x)$

Proof:

$$\begin{aligned} \hat{R}_{ff}^{(i)}(\xi) &= \langle \hat{f}^{(i)}(x + \xi) \hat{f}^{(i)}(x) \rangle_L = \frac{1}{L} \int_0^L \hat{f}^{(i)}(x + \xi) \hat{f}^{(i)}(x) dx \\ &= \frac{1}{L} \int_0^L \sum_{n=1}^N \sum_{m=1}^N \sqrt{\lambda_n} \sqrt{\lambda_m} \xi_n^{(i)} \xi_m^{(i)} \phi_n(x + \xi) \phi_m(x) dx = \frac{1}{L} \sum_{n=1}^N \sum_{m=1}^N \sqrt{\lambda_n} \sqrt{\lambda_m} \xi_n^{(i)} \xi_m^{(i)} \int_0^L \phi_n(x + \xi) \phi_m(x) dx \end{aligned}$$

$$\begin{aligned} \lim_{L \rightarrow \infty} \langle \hat{f}^{(i)}(x + \xi) \hat{f}^{(i)}(x) \rangle_L &= \lim_{L \rightarrow \infty} \left[\frac{1}{L} \sum_{n=1}^N \sum_{m=1}^N \sqrt{\lambda_n} \sqrt{\lambda_m} \xi_n^{(i)} \xi_m^{(i)} \int_0^L \phi_n(x + \xi) \phi_m(x) dx \right] \\ &= \sum_{n=1}^N \sum_{m=1}^N \sqrt{\lambda_n} \sqrt{\lambda_m} \xi_n^{(i)} \xi_m^{(i)} \lim_{L \rightarrow \infty} \left[\frac{1}{L} \int_0^L \phi_n(x + \xi) \phi_m(x) dx \right] \\ &\neq R_{ff}^T(\xi) = \sum_{n=1}^N \lambda_n \phi_n(x + \xi) \phi_n(x) \quad \text{even in the case } n=m \end{aligned}$$

- ✓ K-L sample functions: in general not ergodic in autocorrelation

• Solution of Fredholm integral equation

- ✓ Exact solution feasible only for simple geometries (line, square, circle) and special forms of $C_{ff}(x_1, x_2)$
- ✓ Two main categories of numerical methods are available: integration formulae-based methods (e.g. quadrature method) and expansion methods (e.g. Galerkin)
- ✓ Numerical solution with the conventional Galerkin approach \longrightarrow **Dense** matrices very costly to compute and invert
- ✓ An efficient numerical solution of the Fredholm integral equation is indispensable especially when higher order eigenpairs are needed for an accurate representation of the stochastic field

The wavelet-Galerkin method

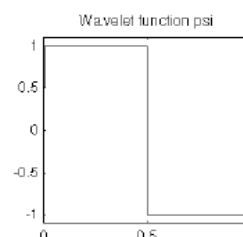
- ✓ Wavelet basis functions enhance the performance of the Galerkin method in the solution of integral equations (Phoon et al. 2002)
- ✓ If the kernel of the integral equation $C_{ff}(x_1, x_2)$ is a rapidly decreasing function, the application of the wavelet-Galerkin method leads to **sparse** matrices (Beylkin, Coifman & Rokhlin 1991)

Basic steps of the wavelet-Galerkin approach:

1. Selection of a set of M wavelet basis functions $\psi_1(x), \psi_2(x), \dots, \psi_M(x)$

Usually Haar wavelets are used (the simplest form of Daubechies wavelets)

Haar mother wavelet function:
$$\psi(x) = \begin{cases} 1 & 0 \leq x < 0.5 \\ -1 & 0.5 \leq x < 1 \\ 0 & \text{otherwise} \end{cases}$$



2. Approximation of each eigenfunction of the covariance kernel by a linear combination of Haar wavelet basis functions:

$$\phi_n(x) = \sum_{i=0}^{M-1} d_i^{(n)} \psi_i(x) = \Psi^T(x) D^{(n)} \quad \begin{array}{l} d_i^{(n)}: \text{wavelet coefficients} \\ M = 2^m, \quad m: \text{wavelet level} \end{array}$$

Remark 1. Number of terms in the truncated K-L expansion: $N \leq M$

3. Solution of the generalized eigenvalue problem: $\Psi^T(x) \Lambda D = \Psi^T(x) A H D$

Remark 2. A crucial difference of this approach with the conventional Galerkin method: the computation of matrices A and H does **not** require numerical integration

Matrix A is the 2D wavelet transform of $C_{ff}(x_1, x_2)$ and H a diagonal MxM matrix

Remark 3. Matrix A is sparse by nature and can be made further sparse by ignoring elements below a threshold value \rightarrow This may lead to computational instabilities in the numerical procedure

• Numerical examples (Stefanou & Papadrakakis 2007)

1. First order Markov stochastic field with exponential covariance function

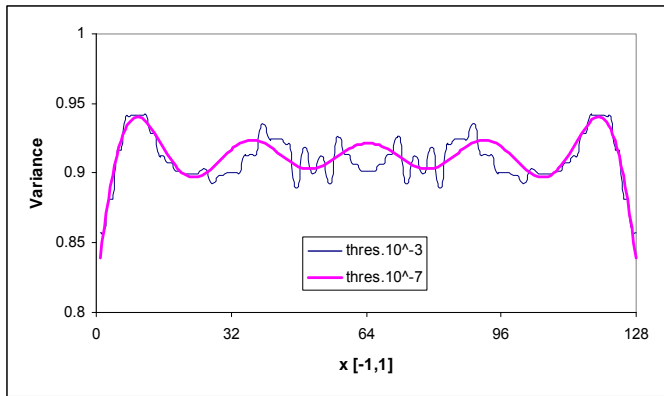
$$\text{Case 1: } C_{ff}(\xi) = R_{ff}(\xi) = \sigma^2 e^{-|\xi|/b} \Rightarrow S_{ff}(\kappa) = \frac{\sigma^2}{\pi} \frac{b}{(1+b^2\kappa^2)} \quad \begin{array}{l} \text{- zero mean, unit variance} \\ \text{- selected threshold values in step 3: } 10^{-3}, 10^{-7} \end{array}$$

2. Stochastic field with square exponential covariance function

$$\text{Case 2: } C_{ff}(\xi) = R_{ff}(\xi) = \sigma^2 e^{-\xi^2/b^2} \Rightarrow S_{ff}(\kappa) = \frac{\sigma^2 b}{2\sqrt{\pi}} \exp\left(-\frac{b^2\kappa^2}{4}\right) \quad \begin{array}{l} \text{- zero mean, unit variance} \\ \text{- selected threshold value in step 3: } 10^{-12} \end{array}$$

✓ A smaller threshold value is selected for case 2 because the square exponential kernel is sparser by its nature

✓ Parameters: Wavelet level $m=7$ ($M=2^7=128$ eigenpairs can be computed at most), number of K-L terms-points in the discretization of the wave number domain $N=16$, number of terms in the FFT series $M=128$



Ensemble variance of truncated K-L expansion:

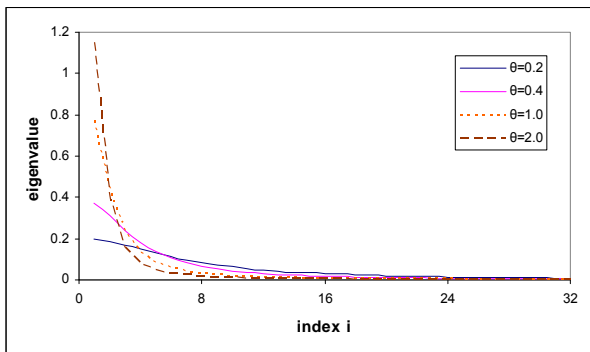
$$\text{Var}[\hat{f}(x)] = \sum_{n=1}^N \lambda_n \phi_n^2(x)$$

- Wavelet level $m = 7$
- Threshold values in matrix A: $10^{-3}, 10^{-7}$

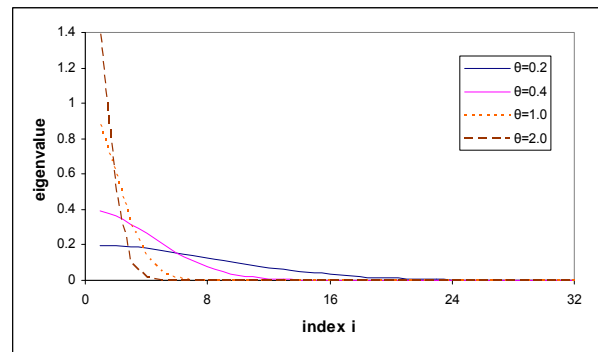
✓ Mean variance: 0.912
Good approximation for 5 K-L terms

- ✓ The variance is fluctuating w.r.t. x
- ✓ The error at the boundaries is larger compared to the middle region

- ✓ Threshold value 10^{-3} : substantial oscillations observed throughout the range $[-1,1]$ due to the numerical instabilities in the calculation of eigenpairs
- ✓ Threshold value 10^{-7} : a stable solution is obtained

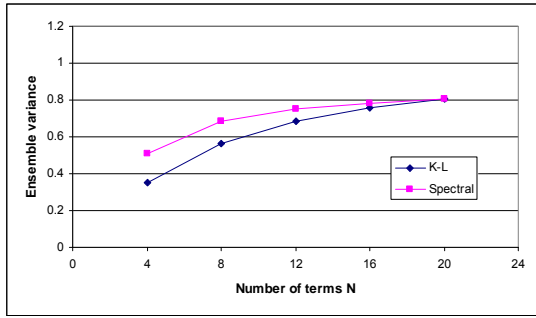


Case 1: $\theta = 2b$

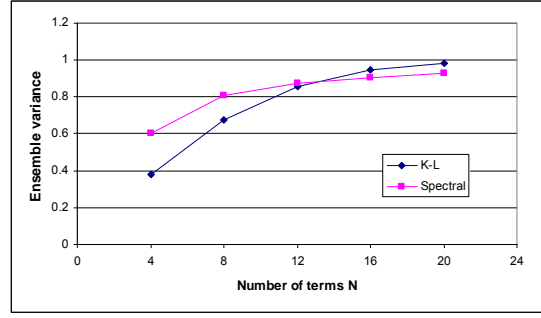


Case 2: $\theta = \sqrt{\pi}b$

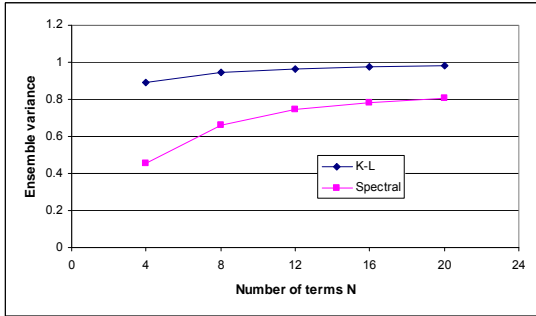
- Eigenvalue decay for $\theta=0.2, 0.4, 1.0$ and 2.0 (θ : Vanmarcke's scale of fluctuation)
- ✓ The most rapid eigenvalue decay is observed in case 2 for $\theta=2.0$ (strongly correlated stochastic field with smooth autocovariance function)
- ✓ Few K-L terms are needed for an accurate simulation of random fields of this kind



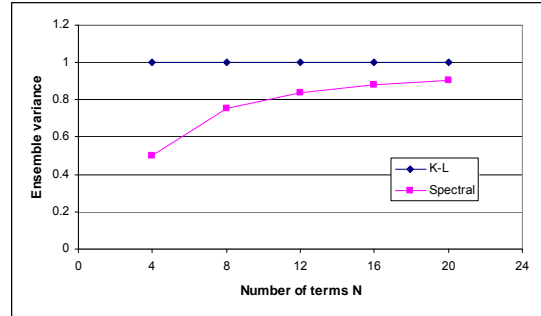
Case 1: $\theta=0.2$



Case 2: $\theta=0.2$



Case 1: $\theta=2.0$



Case 2: $\theta=2.0$

Convergence of each approach to the target variance

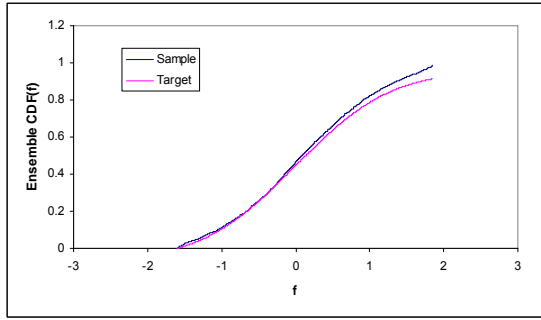
Samples generated with the K-L expansion ($N=16, \theta=0.2$)				
	Worst	Best	Average	Target
Min. value	-3.3076	-2.0820	-1.7178	
Max. value	1.1902	1.7706	1.5981	
Mean	-0.3434	-0.1370	-0.0115	0.000
Variance	0.8954	0.7032	0.6791	1.000
Skewness	-1.1962	0.0153	-0.0761	0.000
Samples generated with the spectral representation ($N=16, \theta=0.2$)				
	Worst	Best	Average	Target
Min. value	-1.3331	-1.9034	-1.9070	
Max. value	3.2233	1.8684	2.0226	
Mean	0.0000	0.0000	0.0000	0.000
Variance	0.7848	0.7848	0.7848	1.000
Skewness	1.6556	-0.0103	0.0711	0.000

Case 1

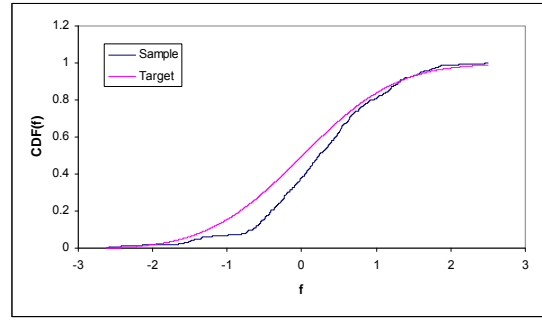
Samples generated with the K-L expansion ($N=16, \theta=0.2$)				
	Worst	Best	Average	Target
Min. value	-1.5411	-1.7148	-1.5988	
Max. value	1.9598	1.8932	1.8455	
Mean	0.5846	0.0813	0.0872	0.000
Variance	0.5237	0.8803	0.7592	1.000
Skewness	-0.5614	0.0166	0.0595	0.000
Samples generated with the spectral representation ($N=16, \theta=0.2$)				
	Worst	Best	Average	Target
Min. value	-1.2252	-2.3388	-1.9791	
Max. value	3.4019	2.1147	2.0328	
Mean	0.0000	0.0000	0.0000	0.000
Variance	0.9069	0.9069	0.9069	1.000
Skewness	1.7822	-0.0004	0.0678	0.000

Case 2

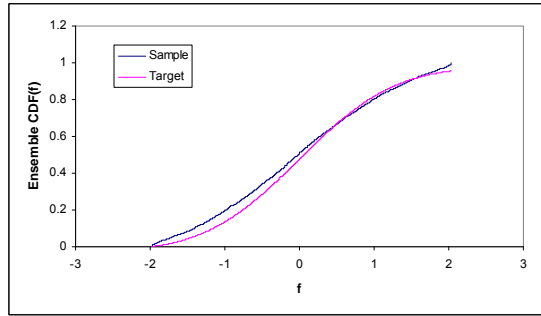
✓ Spectral representation produces ergodic sample functions in a sample-by-sample sense i.e. every sample function has the target mean and SDF (see below SDF plots)



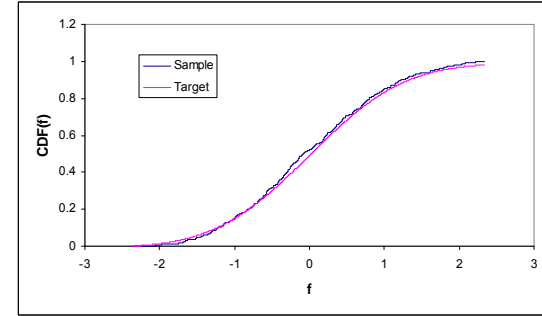
K-L expansion: ensemble average



K-L expansion: Case 1, $\theta=0.2, m=9$

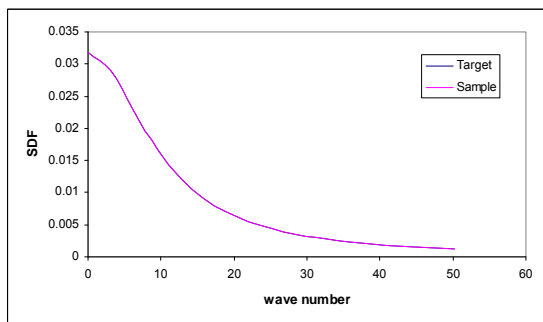


Spectral representation: ensemble average

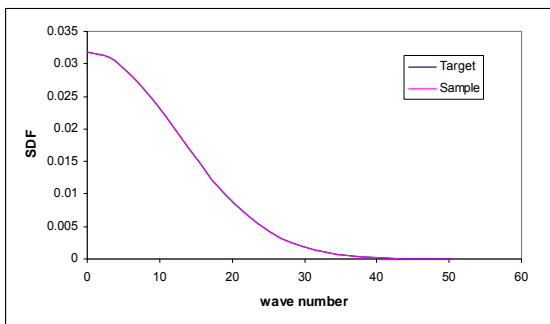


Spectral representation: Case 1, $\theta=0.2, m=9$

Case 2
 $\theta=0.2$



Case 1



Case 2

Ergodicity of spectral representation-based samples with regard to SDF: a perfect matching of the target SDF is observed (cases 1-2, $\theta=0.2$)

$$S_{ff}^{(i)}(\kappa) = \left| \frac{1}{2\pi T_0} \int_0^{T_0} \hat{f}^{(i)}(x) \exp(-i\kappa x) dx \right|^2$$

Wavelet level, power in FFT series (m)	7	9
K-L expansion (1 sample)	2.5	60.0
Spectral representation (1 sample)	3×10^{-4}	10^{-3}

Computational performance of K-L expansion and spectral representation

Simulation of non-Gaussian stochastic fields

Theoretically all the joint multi-dimensional density functions are needed to fully characterize a non-Gaussian stochastic field



Much of the existing research has focused on a more realistic way of defining a non-Gaussian sample function e.g. as a **simple transformation** of some underlying Gaussian field with known second-order statistics:

➤ **Translation field theory** (Grigoriu 1984, 1998): $f(x) = F^{-1} \cdot \Phi[g(x)]$

- Spectral distortion: $S_{ff}(\kappa) \neq S_{ff}^T(\kappa)$

- Compatibility of F - $R_{ff}^T(\xi)$: $R_{ff}^T(\xi) = E[f(x)f(x+\xi)] = E \left\{ \underset{F^{-1}\Phi}{h[g(x)]} \underset{F^{-1}\Phi}{h[g(x+\xi)]} \right\} \Rightarrow$

$$R_{ff}^T(\xi) = \int_{-\infty}^{\infty} \int_{-\infty}^{\infty} F^{-1}[\Phi(g_1)]F^{-1}[\Phi(g_2)] \cdot \phi[g_1, g_2; R_{gg}(\xi)] dg_1 dg_2$$

where $g_1 = g(x)$, $g_2 = g(x + \xi)$

and $\phi[g_1, g_2; R_{gg}(\xi)]$ the joint density of $\{g_1, g_2\}$

• Characteristics of translation fields

- ✓ The relationship between the two autocorrelation functions can have a closed form only in few cases
- ✓ Strictly speaking, if the target F and $R_{ff}^T(\xi)$ are proven to be incompatible, there is no translation field with the prescribed characteristics.
- ✓ The problem of incompatibility becomes even greater for highly skewed narrow-banded stochastic fields (Grigoriu 1998)
- ✓ Analytical expressions of crossing rates are available for translation fields

- In order to address the problem of spectral distortion → Iterative methods (e.g. Yamazaki-Shinozuka 1988, Deodatis-Micaletti 2001)

Repeated updating of $S_{gg}(\kappa)$ in every iteration: $S_{gg}^{(j+1)}(\kappa) = \left[\frac{S_{ff}^T(\kappa)}{S_{ff}^{(j)}(\kappa)} \right]^\alpha S_{gg}^{(j)}(\kappa)$

Unwanted correlations between the terms of the spectral representation series

After the first iteration, the underlying Gaussian field is no more Gaussian and homogeneous. Finally, the generated non-Gaussian sample functions will not have the prescribed marginal PDF

Use of extended non-Gaussian to non-Gaussian mapping: $f(x) = F^{-1} \cdot F^*[g(x)]$

- To address the issue of possible incompatibility between F and $R_{ff}^T(\xi)$: Spectral preconditioning → Generated non-Gaussian field: **approximately** translation field

- Correlations between the terms of the spectral representation series (proof):

$$g_0^{(j+1)}(x) = 2 \sum_{n=0}^{N-1} \sqrt{S_{gg}^{(j+1)}(\kappa_n)} \Delta \kappa \cos(\kappa_n x + \phi_n) \quad \text{in iteration } j+1$$

$$S_{ff}^{(j)}(\kappa) = \left| \frac{1}{2\pi T} \int_0^T f_0^{(j)}(x) \exp(-i\kappa x) dx \right|^2 = \left| \frac{1}{2\pi T} \int_0^T F^{-1} \Phi[g_0^{(j)}(x)] \exp(-i\kappa x) dx \right|^2$$

$$= \left| \frac{1}{2\pi T} \int_0^T F^{-1} \Phi \left[2 \sum_{n=0}^{N-1} \sqrt{S_{gg}^{(j)}(\kappa_n)} \Delta \kappa \cos(\kappa_n x + \phi_n) \right] \exp(-i\kappa x) dx \right|^2$$

✓ $S_{ff}^{(j)}(\kappa)$ depends on the random phase angles ϕ_n

$$\Downarrow S_{gg}^{(j+1)}(\kappa) = \left[\frac{S_{ff}^T(\kappa)}{S_{ff}^{(j)}(\kappa)} \right]^\alpha S_{gg}^{(j)}(\kappa)$$

✓ $S_{gg}^{(j+1)}(\kappa)$ also depends on the random phase angles ϕ_n → alteration of the marginal PDF of $g_0^{(j+1)}(x)$ due to c.l.t.

➤ Proposed enhanced hybrid method (Lagaros, Stefanou & Papadrakakis 2005)

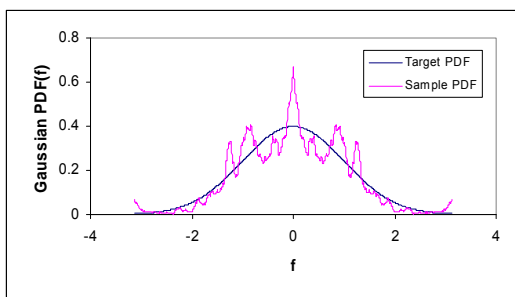
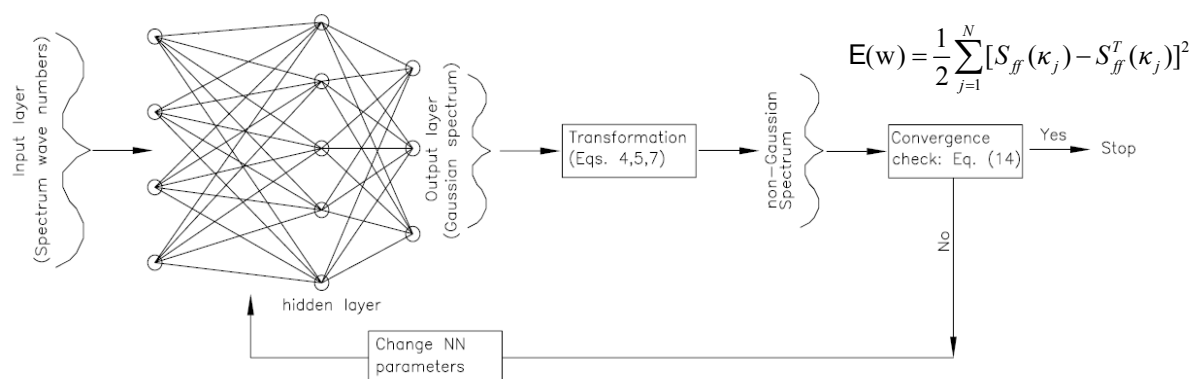
Basic idea: replace the updating scheme of the Gaussian spectrum $S_{gg}(\kappa)$ (source of all important difficulties in the simulation) by a NN-based regression model

✓ The unwanted correlations between the terms of the spectral representation series become negligible

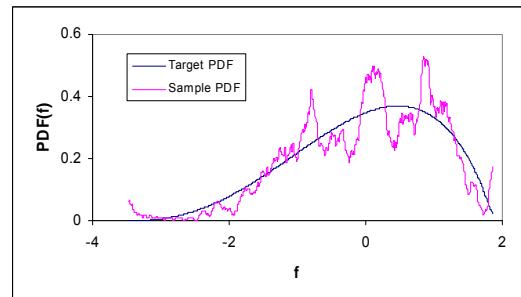
✓ Use of the extended mapping: $f(x) = F^{-1} \cdot F^*[g(x)]$

✓ Spectral preconditioning is not required → an algorithm covering a **wider** range of non-Gaussian fields is obtained (not only translation fields).

✓ A very small number (<50) of iterations is required until convergence → drastic reduction of the computational effort required for simulation



Exact and sample Gaussian PDF at first iteration



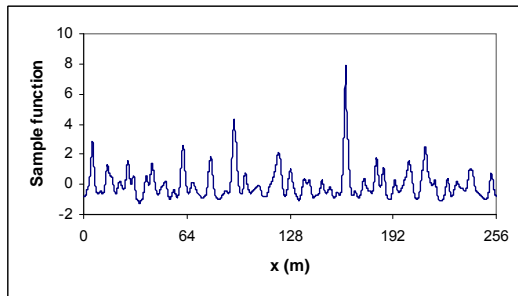
Exact and sample beta PDF at final iteration (translation field case)

- Numerical example: a highly skewed narrow-banded stochastic field

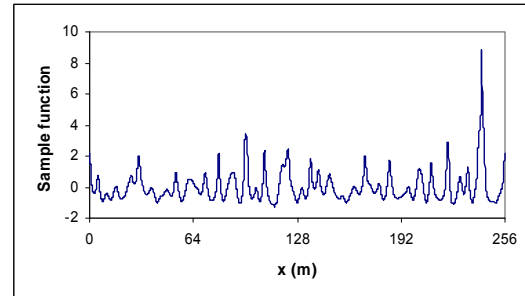
Characteristics of target non-Gaussian field:

- Lognormal distribution defined in the range [-1.30, 10.0] → skewness $\gamma = 2.763$, kurtosis $\delta = 19.085$

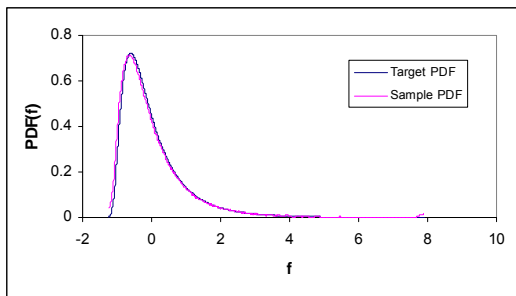
- Target correlation structure: $S_{ff}^T(\kappa) = \frac{1}{4} \sigma^2 b^3 \kappa^2 \exp[-b|\kappa|]$ $\sigma = 1$ και $b = 5$



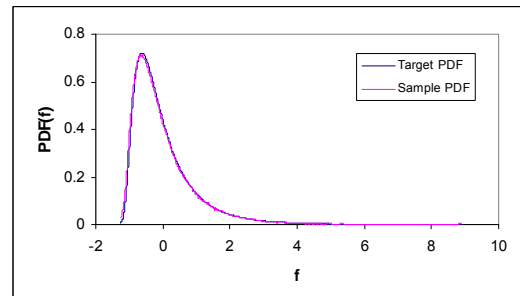
Sample function generated using the D-M algorithm: [-1.23, 7.87]



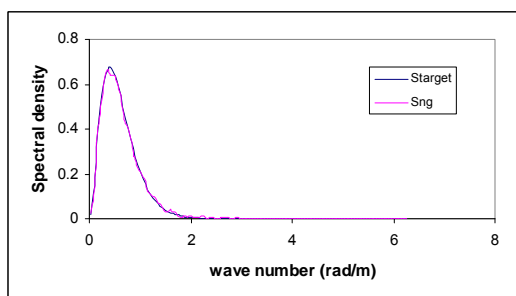
Sample function generated using the proposed EHM: [-1.25, 8.89]



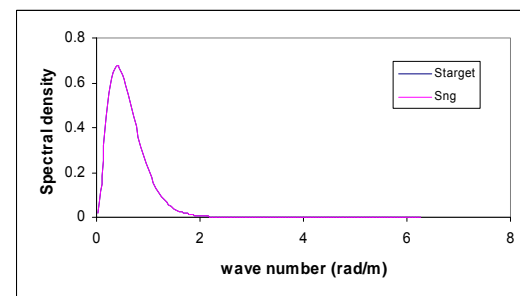
Marginal PDF of sample function generated using the D-M algorithm versus target lognormal PDF



Marginal PDF of sample function generated using the proposed EHM versus target lognormal PDF



SDF of sample function generated using the D-M algorithm versus target SDF



SDF of sample function generated using the proposed EHM versus target SDF

- ✓ Perfect matching of the target PDF due to the (exact) extended mapping
- ✓ Perfect matching of the target SDF achieved by the proposed EHM (use of Rprop training, Riedmiller & Brown 1993)

Computational performance of D-M and proposed algorithm (EHM)

Method	Iterations	Time (sec)
D-M*	29279	146
EHM-SD	82	2.0
EHM-CG	25	0.6
EHM-Quickprop	45	1.2
EHM-Rprop	32	0.8

✓ Substantially smaller cost of proposed EHM (~ 2 orders of magnitude)



✓ Reduction of cost for the stochastic analysis of realistic structures with uncertain non-Gaussian properties

* : without spectral preconditioning

Statistical comparison of D-M and EHM algorithms

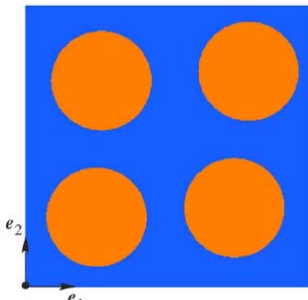
D-M* (Iterations)	EHM-Rprop (Iterations)
29279	32
46843	38
4414	28
24335	29
5935	31
94494	35
53295	33
10628	29
61618	28
51582	29

D-M*
Mean value: 38242
St. dev.: 28701
Max: 94494
Min: 4414

EHM-Rprop
Mean value: 31.2
St. dev.: 3.5
Max: 38
Min: 28

* : without spectral preconditioning

➤ Identification of random shapes from images based on polynomial chaos expansion (Stefanou, Noy & Clement 2009)

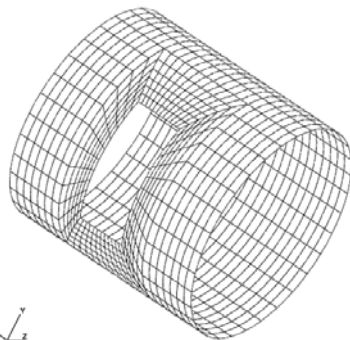


Material layout of a quadratic microstructure

✓ Physical problems with random geometry: disordered systems and random media, fluctuating domain boundaries, shells with cut-outs, heterogeneous materials with random distribution of inclusions...

✓ Usually a limited number of samples of the geometry is available in practice: its complete probabilistic characterization (in terms of joint densities) is infeasible

✓ Shape recovery from simple images allows obtaining many samples at a low cost + it is relatively precise



Cylindrical shell with rectangular cut-out

4/6/2009

IFMA Seminar, France

29

• Short description of the procedure

- Shape recovery with the **level-set** technique: construction of a collection of discretized level-set functions corresponding to a collection of images
- Reduction of information through empirical **Karhunen-Loève expansion**:

$$\phi^{(k)} \approx \mu_\phi + \sum_{i=1}^m \tilde{U}_i X_i^{(k)}$$

- Probabilistic identification of random vector $\mathbf{X} = (X_1, \dots, X_m)$ from samples $\mathbf{X}^{(k)}$ decomposition on a **polynomial chaos** basis of degree p in dimension m (Wiener 1938):

$$\mathbf{X} \approx \sum_{\alpha \in \mathcal{S}_{m,p}} \mathbf{X}_\alpha H_\alpha(\xi(\theta))$$

- Identification of chaos coefficients:

1. **Without** independence hypothesis: maximum likelihood estimation for random vector \mathbf{X}
2. **With** independence hypothesis: maximum likelihood estimation for each random variable or projection method based on empirical CDF

4/6/2009

IFMA Seminar, France

30

The stochastic finite element method

➤ Solution of stochastic elliptic boundary value problems

$$\begin{aligned}
 (\Theta, \mathfrak{I}, P) \quad & \boxed{-\nabla \cdot [\kappa(\mathbf{x}, \theta) \nabla u(\mathbf{x}, \theta)] = f(\mathbf{x}, \theta),} & \mathbf{x} \in D \\
 u : D \times \Theta \rightarrow \mathbb{R} \quad & \boxed{u(\mathbf{x}, \theta) = 0,} & \mathbf{x} \in \partial D
 \end{aligned}$$

- Well posed problem (existence and uniqueness of solution):

✓ $\kappa \in C^1(\bar{D})$

✓ $0 < \kappa_{\min} < \kappa_{\max} \quad \mathbf{KAI} \quad \Pr[\kappa(x, \theta) \in [\kappa_{\min}, \kappa_{\max}], \forall x \in \bar{D}] = 1$

- Weak form: $A(u, v) = B(v) \quad \forall v \in X = H_0^1(D)$

deterministic

$$A(u, v) = \int_D \kappa \nabla u \cdot \nabla v d\mathbf{x}, \quad B(v) = \int_D f v d\mathbf{x} \quad u, v \in X$$

$$\boxed{\langle A(u, v) \rangle = \langle B(v) \rangle} \quad \forall v \in X \otimes L_p^2(\Theta)$$

stochastic

- Finite element approximation → selection of suitable function spaces

e.g. $X^h = \text{span}\{\phi_1, \phi_2, \dots, \phi_{N_x}\} \subset X$ and $W^h = \text{span}\{\psi_1(\xi), \psi_2(\xi), \dots, \psi_{N_\xi}(\xi)\} \subset W$
 $\xi = (\xi_1, \dots, \xi_M)$

➤ 3D elasticity problem:

Formulation of the stochastic stiffness matrix

- Case of material randomness: $D(x, y, z) = D_0 [1 + f(x, y, z)] \rightarrow$

$$\boxed{k^{(e)} = \int_{V^{(e)}} B^{(e)T} D_0^{(e)} B^{(e)} dV^{(e)} + \int_{V^{(e)}} B^{(e)T} D_0^{(e)} B^{(e)} f^{(e)}(x, y, z) dV^{(e)}} \rightarrow \boxed{k^{(e)} = k_0^{(e)} + \Delta k^{(e)}}$$

- Discretization of the stochastic fields

- Midpoint method

- Local average method: $\boxed{k^{(e)} = k_0^{(e)} (1 + a^{(e)})}$

- Weighted integral method: $\boxed{k^{(e)} = k_0^{(e)} + \sum_{l=1}^{N_W} X_l^{(e)} \Delta k_l^{(e)}}$

➤ Response variability calculation

- **Direct Monte Carlo Simulation** (e.g. Rubinstein 1981)

$$E(u_i) = \frac{1}{NSIM} \sum_{j=1}^{NSIM} u_i(j)$$

$$\sigma^2(u_i) = \frac{1}{NSIM - 1} \left[\sum_{j=1}^{NSIM} u_i^2(j) - NSIM \cdot E^2(u_i) \right]$$

- ✓ Solution of *NSIM* deterministic problems → substantial computational cost especially for high dimensional problems and for large number of simulations
- ✓ It must be combined with efficient discretization methods (e.g. local average method)
- ✓ Particularly suitable for parallel computing environment (“embarrassingly parallel”)
- ✓ Assisted by the spectacular growth of computing power, the only available method for the solution of large-scale realistic problems

- **The perturbation method** (Kleiber & Hien 1992)

- ✓ Taylor series expansion of the stochastic finite element matrix and of the resulting response vector:

$$K = K_0 + \sum_{i=1}^N K_i^I a_i + \frac{1}{2} \sum_{i=1}^N \sum_{j=1}^N K_{ij}^{II} a_i a_j + \dots \quad K_i^I = \left. \frac{\partial K}{\partial a_i} \right|_{a=0}, \quad K_{ij}^{II} = \left. \frac{\partial^2 K}{\partial a_i \partial a_j} \right|_{a=0}$$

$$u = u_0 + \sum_{i=1}^N u_i^I a_i + \frac{1}{2} \sum_{i=1}^N \sum_{j=1}^N u_{ij}^{II} a_i a_j + \dots$$

$$u_0 = K_0^{-1} P_0$$

- ✓ Calculation of the stochastic displacement vector:

$$u_i^I = K_0^{-1} (P_i^I - K_i^I u_0)$$

$$u_{ij}^{II} = K_0^{-1} (P_{ij}^{II} - K_i^I u_j^I - K_j^I u_i^I - K_{ij}^{II} u_0)$$

- ✓ Satisfactory results only for small coefficients of variation of the uncertain input parameters
- ✓ Improvement in accuracy obtained using higher order approximations: small compared to the disproportional increase of computational effort

- **The spectral stochastic finite element method** (Ghanem & Spanos 1991)

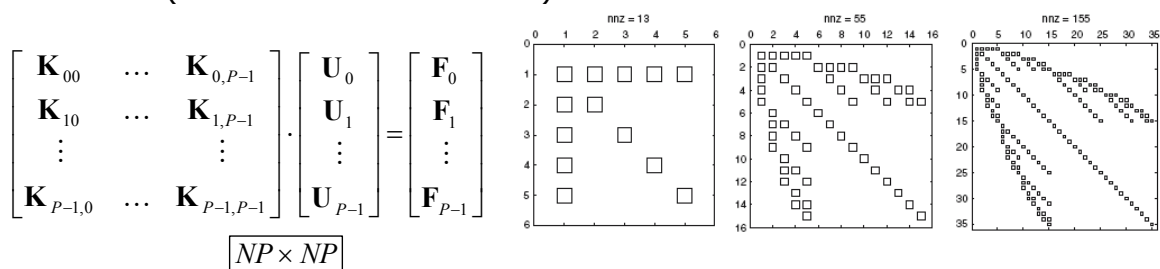
✓ Karhunen-Loève expansion of the stiffness matrix + polynomial chaos expansion (PCE) of the displacement vector:

$$\mathbf{k}^{(e)}(\theta) = \mathbf{k}_0^{(e)} + \sum_{l=1}^M \mathbf{k}_l^{(e)} \xi_l(\theta), \quad \mathbf{k}_i^{(e)} = \sqrt{\lambda_i} \int_{\Omega_e} \phi_i(\mathbf{x}) \mathbf{B}^T \mathbf{D}_0 \mathbf{B} d\Omega_e$$

$$\mathbf{U}(\theta) = \sum_{j=0}^{P-1} \mathbf{U}_j \Psi_j(\theta), \quad P+1 = \frac{(M+p)!}{M!p!}$$

✓ Application (mainly) to linear problems with small variability + Gaussian assumption for the uncertain input parameters (Sudret & der Kiureghian 2002)

✓ Prohibitive computational cost for the solution of problems with large stochastic dimension (increase of the order of PCE)



- Spectral SFEM: recent advances and extensions

✓ Cases of non-smooth solutions (non-linearities, discontinuities): use of other basis functions e.g. wavelets (Le Maitre et al. 2004) or adaptive sparse generalized PCE (Wan & Karniadakis 2005, Blatman & Sudret 2008).

✓ Stochastic reduced basis methods (Nair et al. 2002-2008): limited to random linear systems

✓ Non-intrusive, stochastic response surface approaches (Baroth et al. 2006, Berveiller et al. 2006): can take advantage of powerful deterministic FE codes

✓ Spectral SFEM in a multi-scale setting (Xu 2007): stochastic variational approach + scale-bridging multi-scale shape functions

✓ X-SFEM (Nouy et al. 2007-8): implicit representation of complex geometries using random level-set functions

Stochastic finite element analysis of shells

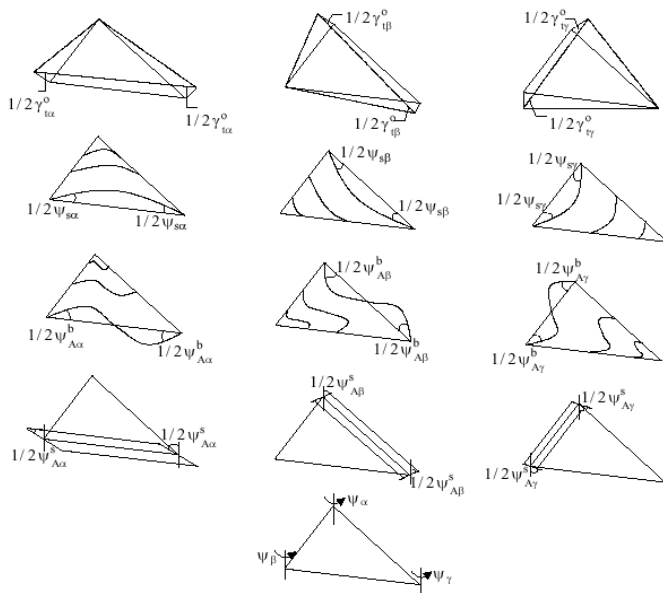
➤ The multi-layered triangular shell element TRIC (Argyris et al. 1997)

- ✓ TRIC is a triangular, shear-deformable facet shell element suitable for the analysis of thin and moderately thick isotropic as well as composite plate and shell structures
- ✓ The element formulation is based on the natural mode finite element method (Argyris et al. 1979)
- ✓ The treatment of the element kinematics eliminates automatically shear locking phenomena (Argyris et al. 2000)
- ✓ No need to perform numerical integration for the computation of the deterministic stiffness matrix which is carried out in closed form → derivation of a cost-effective stochastic stiffness matrix
- ✓ Computational efficiency in large-scale stochastic finite element computations

4/6/2009

IFMA Seminar, France

37



✓ The natural stiffness of the TRIC element is based only on the 12 independent natural straining modes:

$$k_N = \begin{bmatrix} k_{qc} & \mathbf{O} & \mathbf{O} \\ (6 \times 6) & & \\ \mathbf{O} & k_{qh} & \mathbf{O} \\ (3 \times 3) & & \\ \mathbf{O} & \mathbf{O} & k_{az} \\ (3 \times 3) & & \end{bmatrix}$$

k_{qc} : axial and symmetric bending stiffness terms

k_{qh} : anti-symmetric bending and shear stiffness terms

k_{az} : stiffness terms due to in-plane rotations (azimuth stiffness terms)

4/6/2009

IFMA Seminar, France

38

• Derivation of the stochastic stiffness matrix

- Random variation of Young modulus (Argyris, Papadrakakis & Stefanou 2002)

$$E(x, y) = E_0 [1 + f(x, y)]$$

1. $k_{qc} = \int_V B_{ic}^T \kappa_{ct} B_{ic} dV \rightarrow k_{qc} = (1+a)(k_{qc})_0$ ✓ It is proved that the axial and symmetric bending stiffness terms have a local average form

$$a = \frac{1}{\Omega} \int_{\Omega} f(x, y) d\Omega$$

2a. $k_{qh}^b = \int_V B_{th}^T \kappa_{ct} B_{th} dV \rightarrow k_{qh}^b = (k_{qh}^b)_0 + \sum_{i=1}^6 X_i \Delta k_i$

2. $k_{qh} = \left\{ [k_{qh}^b]^{-1} + [k_{qh}^s]^{-1} \right\}^{-1}$ ✓ 6 weighted integrals X_i

2b. $k_{qh}^s = \int_V B_{sh}^T X_s B_{sh} dV \rightarrow k_{qh}^s = (1+a)(k_{qh}^s)_0$

✓ Local average form

e.g. weighted integrals X_1, X_4 : $X_1 = \int_{\Omega} \zeta_a^2 f(\zeta_a, \zeta_{\beta}, \zeta_{\gamma}) d\Omega$ $X_4 = \int_{\Omega} \zeta_a \zeta_{\beta} f(\zeta_a, \zeta_{\beta}, \zeta_{\gamma}) d\Omega$

$\zeta_a, \zeta_{\beta}, \zeta_{\gamma}$ the natural (triangular) coordinates

Matrix Δk_1 of the fluctuating part of the anti-symmetric bending stiffness terms:

$$\Delta k_1 = \begin{bmatrix} 0 & 0 & 0 & -\frac{l_{\beta} l_{\gamma}}{l_a^4} z^2 k_{aa} - \frac{3l_{\gamma}}{l_a^2 l_{\beta}} z^2 k_{a\beta} - \frac{3l_{\beta}}{l_a^2 l_{\gamma}} z^2 k_{a\gamma} - \frac{9}{l_{\beta} l_{\gamma}} z^2 k_{\beta\gamma} \\ \frac{l_{\beta}^2}{l_a^4} z^2 k_{aa} + \frac{6}{l_a^2} z^2 k_{a\beta} + \frac{9}{l_{\beta}^2} z^2 k_{\beta\beta} & & & \\ \text{symm.} & & & \frac{l_{\gamma}^2}{l_a^4} z^2 k_{aa} + \frac{6}{l_a^2} z^2 k_{a\gamma} + \frac{9}{l_{\gamma}^2} z^2 k_{\gamma\gamma} \end{bmatrix}$$

$$z^2 k_{ij} = \int_{-h/2}^{h/2} z^2 \kappa_{ij} dz = \frac{1}{3} \sum_{k=1}^N \kappa_{ij}^k (z_k^3 - z_{k+1}^3) \quad i, j = \alpha, \beta, \gamma$$

- κ_{ij} the entries of the constitutive matrix κ_{ct}
 - $k = 1, 2, \dots, N$ the number of layers

$$3. \quad k_{az} = \begin{bmatrix} k_z^{aa} & k_z^{a\beta} & k_z^{a\gamma} \\ & k_z^{\beta\beta} & k_z^{\beta\gamma} \\ \text{symm} & & k_z^{\gamma\gamma} \end{bmatrix} = k_z \begin{bmatrix} 1 & -0.5 & -0.5 \\ -0.5 & 1 & -0.5 \\ -0.5 & -0.5 & 1 \end{bmatrix}$$

k_z the maximum of the three edge bending stiffness values:

$$k_z = \Omega \cdot \max \left\{ \frac{1}{l_a^2} \int_{-h/2}^{h/2} z^2 \kappa_{aa} dz, \frac{1}{l_\beta^2} \int_{-h/2}^{h/2} z^2 \kappa_{\beta\beta} dz, \frac{1}{l_\gamma^2} \int_{-h/2}^{h/2} z^2 \kappa_{\gamma\gamma} dz \right\}$$

$$\Downarrow \quad k_z^{(i)} = \frac{\Omega}{l_i^2} \int_{-h/2}^{h/2} z^2 \kappa_{ii} dz$$

$$k_z = \max \left\{ (1+a)k_z^{(a)}, (1+a)k_z^{(\beta)}, (1+a)k_z^{(\gamma)} \right\}$$

$$a = \frac{1}{\Omega} \int_{\Omega} f(x,y) d\Omega$$

✓ The azimuth stiffness terms have also an inherent local average form

- Combined random variation of Young modulus and Poisson ratio (Stefanou & Papadrakakis 2004)

✓ The entries of the elasticity matrix are **nonlinear** functions of Poisson ratio → consideration of random variation of Lamé constants λ and μ

$$\kappa_{12} = \frac{E}{1-\nu^2} \begin{bmatrix} 1 & \nu & 0 \\ \nu & 1 & 0 \\ 0 & 0 & 1-\nu \end{bmatrix} \longrightarrow \kappa_{12} = \begin{bmatrix} \lambda + 2\mu & \lambda & 0 \\ \lambda & \lambda + 2\mu & 0 \\ 0 & 0 & 2\mu \end{bmatrix}$$

$$\lambda = \frac{\nu E}{1-\nu^2}$$

$$\mu = G = \frac{E}{2(1+\nu)}$$

$$\lambda(x,y) = \lambda_0 [1 + f_\lambda(x,y)] \quad + \quad \mu(x,y) = \mu_0 [1 + f_\mu(x,y)]$$

- ✓ Axial and symmetric bending stiffness terms: local average form
- ✓ Anti-symmetric bending stiffness terms: 12 weighted integrals
- ✓ Anti-symmetric shear stiffness terms: local average form
- ✓ Azimuth stiffness terms: local average form

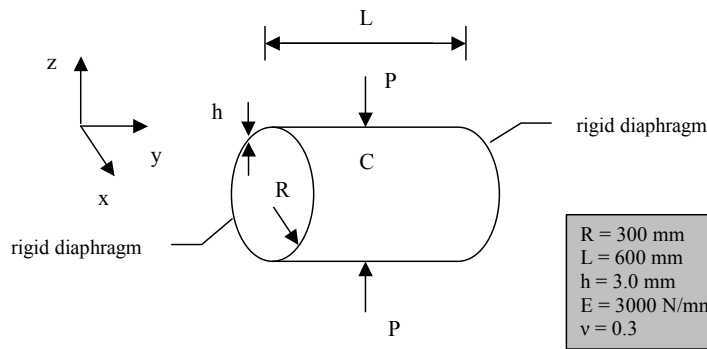
- Random variation of the thickness

✓ The thickness h appears into the integrals expressing the stiffness matrix of the shell element

✓ The application of the weighted integral method is not straightforward →
The local average approach is applied leading to greater computational efficiency

$$h(x, y) = h_0(1 + a_h)$$

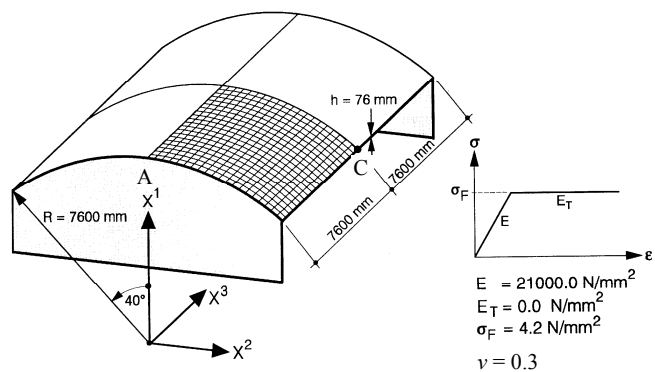
$$a_h = \frac{1}{\Omega} \int_{\Omega} f_h(x, y) d\Omega$$



• Numerical examples
(Stefanou & Papadrakakis 2004)

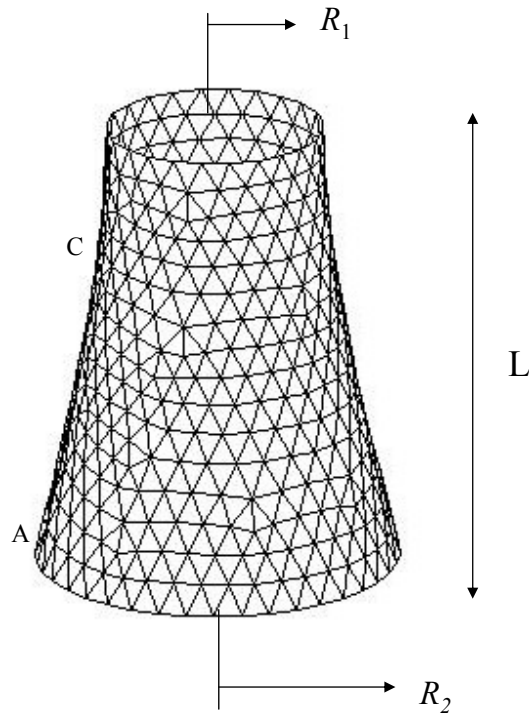
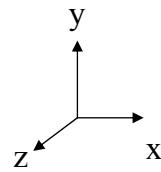
R = 300 mm
L = 600 mm
h = 3.0 mm
E = 3000 N/mm²
ν = 0.3

1. Pinched cylinder



2. Scordelis-Lo shell

$$\begin{aligned}
 R_1 &= 4800 \text{ mm} \\
 R_2 &= 8000 \text{ mm} \\
 L &= 20000 \text{ mm} \\
 h &= 40 \text{ mm} \\
 E &= 21000 \text{ N/mm}^2 \\
 \nu &= 0.25
 \end{aligned}$$



3. Hyperboloid shell

- ✓ Use of 2D homogeneous Gaussian stochastic fields for the representation of the uncertain material and geometric properties
- ✓ Sample functions of the stochastic fields generated by the spectral representation method
- ✓ Selection of two different correlation structures:

$$S_{ff}(\kappa_1, \kappa_2) = \frac{\sigma_f^2}{\pi} b_1 b_2 (b_1^2 \kappa_1^2 + b_2^2 \kappa_2^2) \exp[-(b_1^2 \kappa_1^2 + b_2^2 \kappa_2^2)] \quad [1]$$

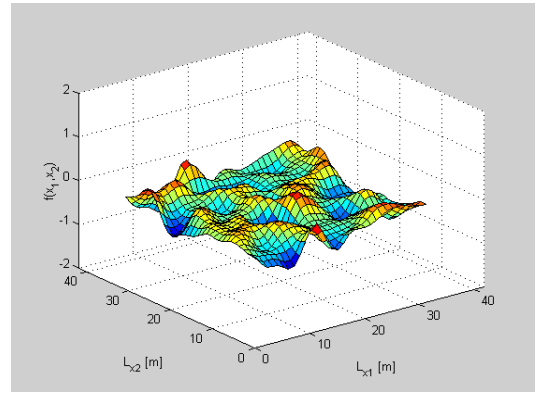
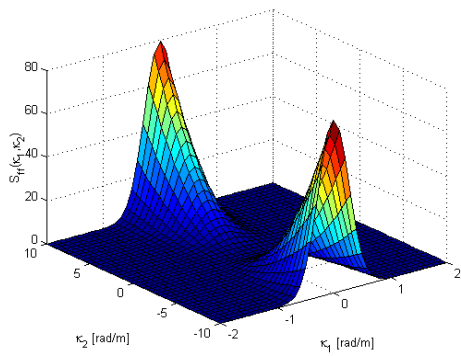
$$S_{ff}(\kappa_1, \kappa_2) = \sigma_f^2 \frac{b_1 b_2}{4\pi} \exp\left[-\left(\frac{b_1 \kappa_1}{2}\right)^2 - \left(\frac{b_2 \kappa_2}{2}\right)^2\right] \quad [2]$$

- ✓ Calculation of COV of displacement at the characteristic node C:

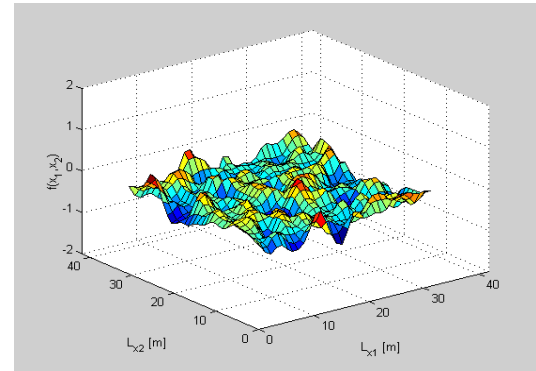
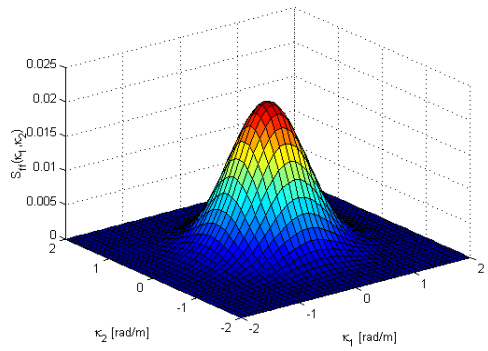
$$COV(u_i) = \frac{\sigma(u_i)}{E(u_i)}$$

- ✓ Investigation of the effect of various parameters of the stochastic fields (σ_f , S_{ff} , b_1 , b_2) on the response variability

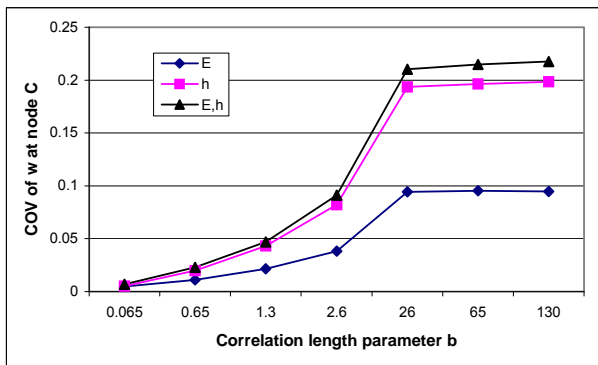
1



2

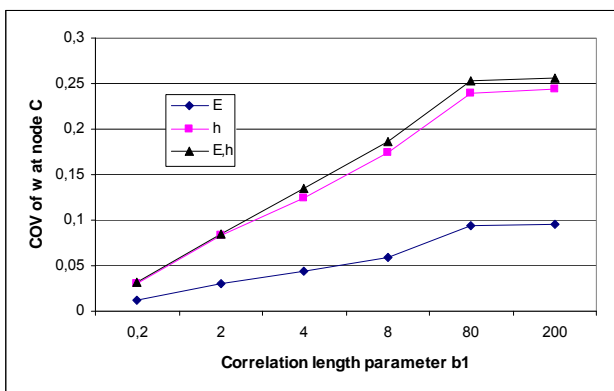


$\sigma_f = 0.2 \quad b_1 = b_2 = 2.6$



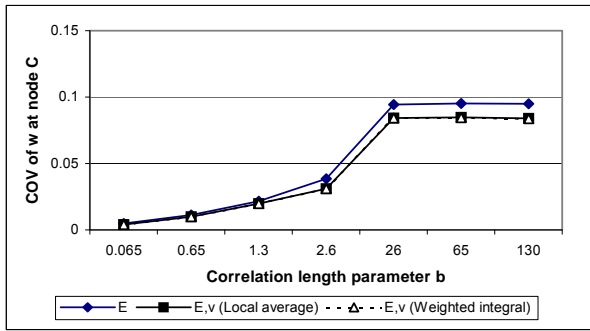
• Scordelis-Lo shell ($\sigma_f = 0.1$):
Random variation of Young modulus and thickness (local average method)

✓ Important effect of thickness variation



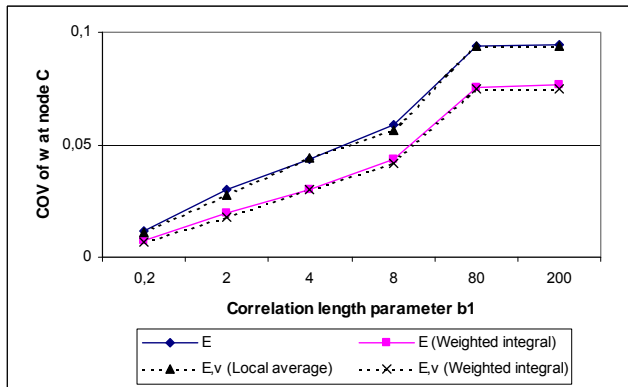
• Hyperboloid shell ($\sigma_f = 0.1$):
Random variation of Young modulus and thickness (local average method)

✓ Important effect of thickness variation



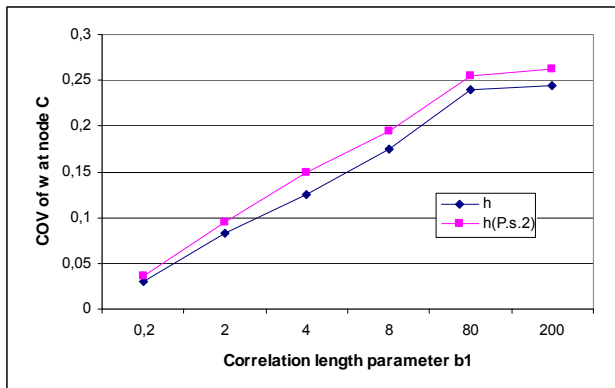
• Scordelis-Lo shell ($\sigma_f = 0.1$):
Random variation of Young modulus
and Poisson ratio

✓ Negligible effect of Poisson ratio
variation



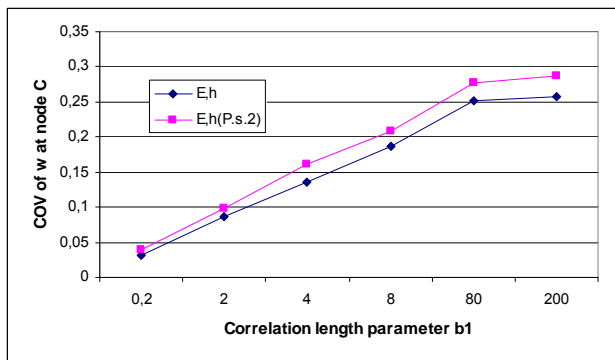
• Hyperboloid shell ($\sigma_f = 0.1$):
Random variation of Young modulus
and Poisson ratio

✓ Negligible effect of Poisson ratio
variation



• Hyperboloid shell ($\sigma_f = 0.1$):
Random variation of Young modulus
and thickness (local average method)

✓ Investigation of the effect of
correlation structure (power spectrum)



$$\text{Var}(w_C) \sim S_{ff}(\kappa)$$

• Conclusions

- ✓ The stochastic stiffness matrix of the TRIC shell element is formulated in terms of a minimum number of random variables
- ✓ Good agreement between weighted integral and local average methods
- ✓ Significant effect of correlation length parameter b on the response variability
- ✓ Slight effect of correlation structure (expressed via the form of the power spectrum) on the response variability
- ✓ Random variation in the shell thickness has significant effect on the response variability compared to the effect of random Young modulus
- ✓ Small effect of random variation of Poisson ratio on the results

Stability analysis of shells with random imperfections

- ✓ Large scatter in the measured buckling loads
 - ✓ Big discrepancy between the deterministic predictions of buckling loads and the corresponding experimental results
- ↓
- ✓ Presence of initial imperfections which occur during the manufacturing and construction stages
 - ✓ Realistic description of imperfections in the framework of a robust stochastic finite element formulation
 - ✓ Importance of available data banks for the realistic simulation of imperfections (estimation of probability distribution, correlation structure), e.g. Elishakoff & Arbocz (1982, 1985)

➤ **Methods based on random variables**

✓ Use of 2D Fourier series with random Fourier coefficients (e.g. Chryssanthopoulos & Poggi 1995, Noirfalise et al. 2007) for the representation of geometric imperfections

✓ This idea is related to the fact that an analytical buckling analysis of cylindrical shells yields a 2D Fourier series representation of the critical modes

➤ **Methods based on stochastic fields**

✓ Simulation of the imperfections using stochastic fields combined with the finite element method for the solution of the stability problem

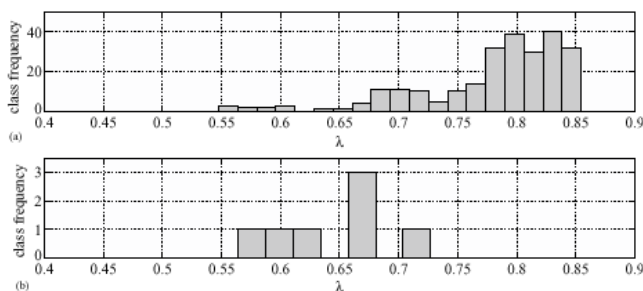
✓ Use of direct Monte Carlo simulation for the computation of buckling load variability

➤ **Stability analysis of cylindrical shells with random geometric imperfections (Schenk & Schueller 2003)**

✓ Use of the data bank by Arbocz & Abramovich (1979) for the estimation of the probability distribution and correlation structure of the imperfections →

✓ Selection of 2D non-homogeneous Gaussian stochastic fields for the description of the imperfections

✓ 250 direct Monte Carlo simulations for the computation of buckling load variability (finite element model with geometric non-linearity)



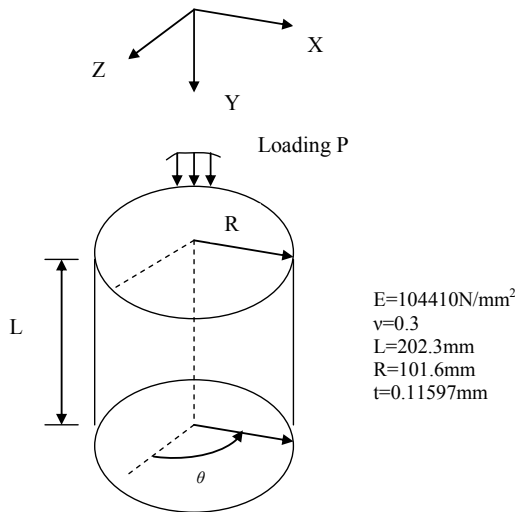
✓ The experimentally determined scatter in the limit load can be predicted numerically



✓ A more accurate prediction requires the incorporation of other kinds of imperfections e.g. material, thickness, boundary conditions

➤ Stability analysis of cylindrical shells with random geometric, material, thickness and boundary imperfections (Papadopoulos, Stefanou & Papadrakakis 2009)

- ✓ Use of TRIC shell element with geometric and material non-linearity
- ✓ Selection of 2D non-homogeneous Gaussian stochastic fields for the description of geometric imperfections (data bank by Arbocz & Abramovich, 1979)
- ✓ Effect of non-Gaussian assumption for E, t on buckling load variability



Randomly varying quantities:

$$r(x, y) = R + a_0(x, y) + g_1(x, y)$$

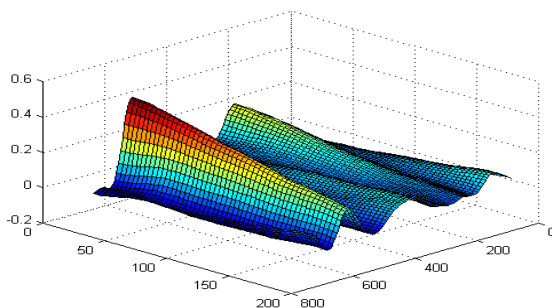
$$E(x, y) = E_0[1 + f_1(x, y)]$$

$$t(x, y) = t_0[1 + f_2(x, y)]$$

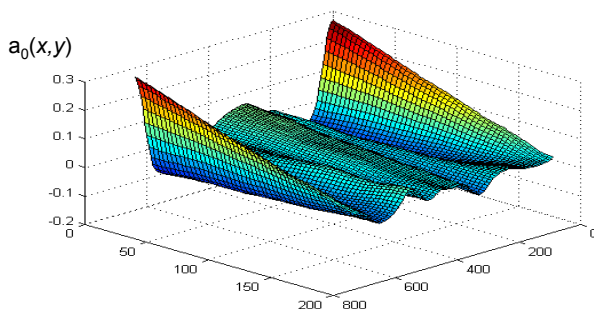
$$P(x) = P_0[1 + g_2(x)]$$

f_1, f_2 : homogeneous non-Gaussian translation fields

- Initial geometric imperfections: $r(x, y) = R + a_0(x, y) + g_1(x, y)$



Measured initial unfolded shape of shell A7



Shell	R(mm)	t (mm)	L (mm)	E (N/mm ²)	P (N)
A-7	101.6	0.1140	203.20	104110	3036.4
A-8	101.6	0.1179	203.20	104800	3673.8
A-9	101.6	0.1153	203.20	101350	3724.8
A-10	101.6	0.1204	203.20	102730	3196.9
A-12	101.6	0.1204	209.55	104800	3853.0
A-13	101.6	0.1128	196.85	104110	3108.8
A-14	101.6	0.1110	196.85	108940	3442.9

Geometry, material properties and experimental buckling loads of A-shells (Arbocz & Abramovich, 1979)

- ✓ The ensemble average $a_0(x, y)$ as well as the evolutionary power spectrum of stochastic field $g_1(x, y)$ are derived from a statistical analysis of experimentally measured imperfections of A-shells

- Material and thickness imperfections: use of non-Gaussian translation fields

	Lower bound	Upper bound	Shape parameters	
Lognormal	-1	$+\infty$	-	-
Beta - Case 1	-0.5	0.5	p=12	q=12
U-beta - Case 2	-0.16	0.16	p=0.8	q=0.8
L-beta - Case 3	-0.13	0.26	p=0.8	q=1.6

$$E(x, y) = E_0[1 + f_1(x, y)]$$

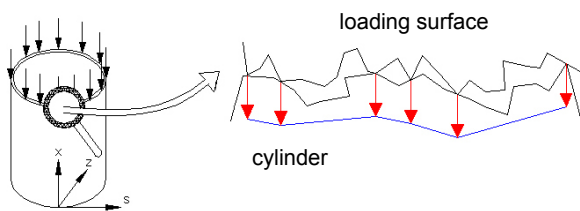
$$t(x, y) = t_0[1 + f_2(x, y)]$$

$$S_{gg}(\kappa_1, \kappa_2) = \sigma_f^2 \frac{b_1 b_2}{4\pi} \exp \left[-\left(\frac{b_1 \kappa_1}{2} \right)^2 - \left(\frac{b_2 \kappa_2}{2} \right)^2 \right]$$

Correlation structure of the imperfections

- In-plane edge (boundary) imperfections: non-uniform axial loading

✓ It is assumed that boundary imperfections are produced by a non-uniform random axial load distribution on the upper edge of the cylinder, modeled as a 1D homogeneous Gaussian stochastic field



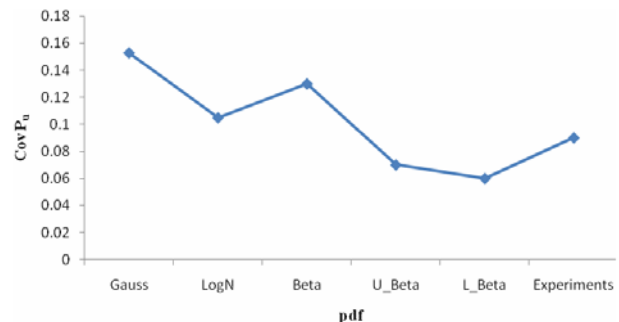
$$P(x) = P_0 [1 + g_2(x)]$$

$$S_{gg}(\kappa) = \frac{\sigma_g^2}{4\pi} b_g \exp \left[-\frac{1}{4} (b_g^2 \kappa^2) \right]$$

- Numerical results

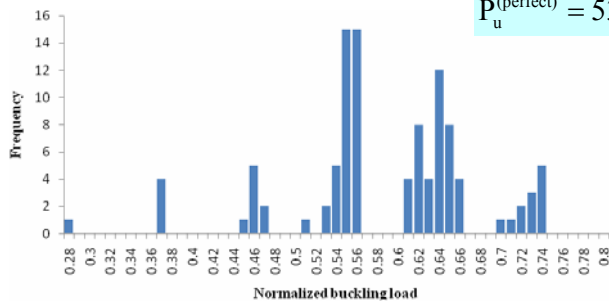
NSIM=100

- ✓ $b_g = 100$ mm with $\sigma_g = 5\%$ are selected for the description of g_2
- ✓ $b_1 = b_2 = 50$ mm with $\sigma_f = 10\%$ are selected for the description of Young modulus and thickness → these values are responsible for the minimum mean(P_U) and it is likely to lead to "worst case" scenarios w.r.t. lowest P_U

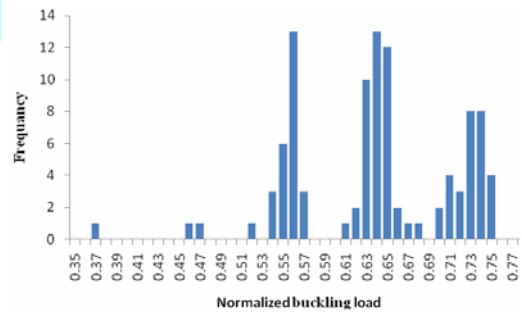


- ✓ The choice of PDF has a significant effect on first and second order properties of P_U distribution
- ✓ Max Cov(=0.16) for a Gaussian PDF, Min Cov(=0.06) for an L-beta PDF

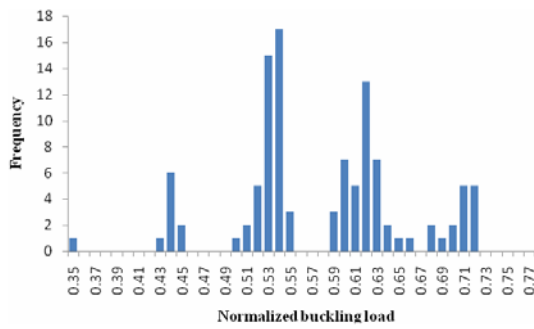
$$P_u^{(\text{perfect})} = 5350\text{N}$$



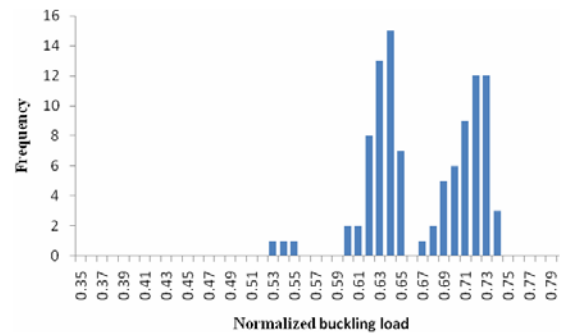
Gaussian E, t



Lognormal E, t



Beta E, t

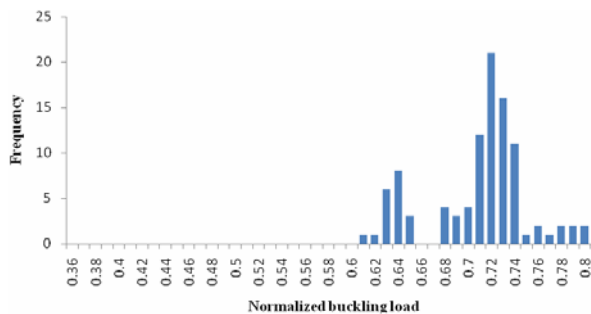


U-beta E, t

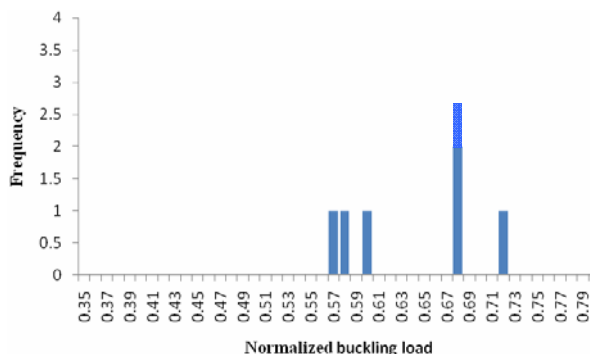
4/6/2009

IFMA Seminar, France

59



L-beta E, t



Experimental

Conclusions

- ✓ The choice of marginal PDF of E, t is crucial: it affects significantly the shape as well as the extreme values of P_u distribution
- ✓ A large magnification of uncertainty has been observed in the Gaussian case: $\text{Cov}(P_u) \sim 1.6\sigma_\epsilon$
- ✓ The lognormal and beta non-Gaussian assumptions led to estimates of the scatter of P_u closer to the experimental measurements
- ✓ The tri-modal shape of buckling loads observed in the experiments has been reproduced by the corresponding numerical simulations
- ✓ The lowest P_u has been found to represent only the 28-60% of the P_u of the perfect shell
- ✓ Towards a robust design of imperfect shell structures

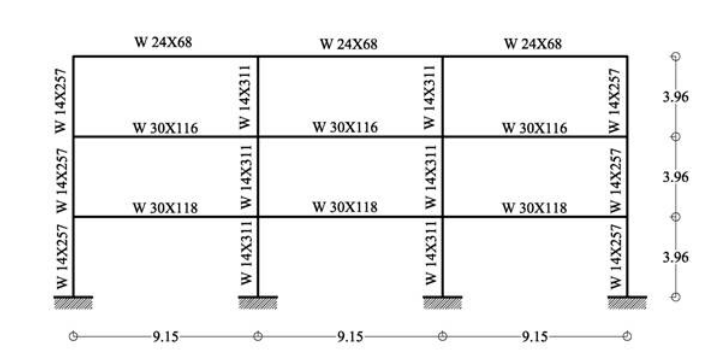
4/6/2009

IFMA Seminar, France

60

Nonlinear stochastic dynamic analysis of frames (Stefanou & Fragiadakis 2009)

- A 3-storey steel moment-resisting frame designed for a Los Angeles site (SAC/FEMA program)
- Fundamental mode period: $T_1=1.02$ sec
- 5 integration sections defined in every beam-column element
- Geometrical nonlinearities not considered in the analysis
- Material law: bilinear with pure kinematic hardening
- Loading: 3 sets of 5 strong ground motion records corresponding to 3 levels of increasing hazard: low, medium and high + spectrum-compatible artificial accelerograms



4/6/2009

IFMA Seminar, France

61

The ground motion records used

ID (level)	Earthquake	Station	ϕ^{o1}	Mw ²	R ³	Soil ⁴	PGA
1 (1/1)	Imperial Valley, 1979	Plaster City	045	6.5	31.7	C,D	0.042
2 (2/1)	Imperial Valley, 1979	Plaster City	135	6.5	31.7	C,D	0.057
3 (3/1)	Imperial Valley, 1979	Westmoreland Fire Station	180	6.5	15.1	C,D	0.11
4 (4/1)	Imperial Valley, 1979	Westmoreland Fire Station	090	6.5	15.1	C,D	0.074
5 (5/1)	Imperial Valley, 1979	Compuertas	285	6.5	32.6	C,D	0.147
6 (1/2)	Northridge, 1994	LA, Baldwin Hills	090	6.7	31.3	B,B	0.239
7 (2/2)	Imperial Valley, 1979	Plaster City	090	6.5	31.7	C,D	0.057
8 (3/2)	Loma Prieta, 1989	Sunnyvale Colton Ave	270	6.9	28.8	C,D	0.207
9 (4/2)	Superstition Hills, 1987	Wildlife Liquefaction Array	090	6.7	24.4	C,D	0.18
10 (5/2)	Loma Prieta, 1989	Sunnyvale Colton Ave	360	6.9	28.8	C,D	0.209
11 (1/3)	Superstition Hills, 1987	Wildlife Liquefaction Array	360	6.7	24.4	C,D	0.2
12 (2/3)	Northridge, 1994	LA, Hollywood Storage FF	360	6.7	25.5	C,D	0.358
13 (3/3)	Loma Prieta, 1989	Hollister South & Pine	000	6.9	28.8	-,D	0.371
14 (4/3)	Loma Prieta, 1989	WAHO	000	6.9	16.9	-,D	0.370
15 (5/3)	Loma Prieta, 1989	WAHO	090	6.9	16.9	-,D	0.638

¹ Component ² Moment magnitude ³ Closest distance to fault rupture

⁴ USGS, Geomatrix soil class

4/6/2009

IFMA Seminar, France

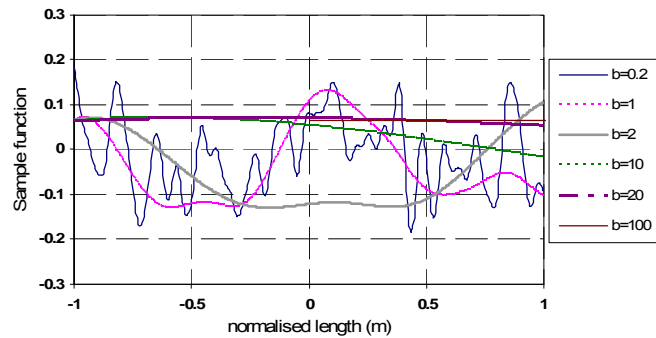
62

	Lower bound	Upper bound	Shape parameters	
Lognormal	-1	$+\infty$	-	-
L-beta	-0.13	0.26	p=0.8	q=1.6

- 1D stochastic variation of Young modulus and yield stress described by zero-mean lognormal and L-beta translation fields with $\sigma_f=10\%$
- The variability of the maximum inter-storey drift θ_{max} is examined using 1000 Monte Carlo simulations:

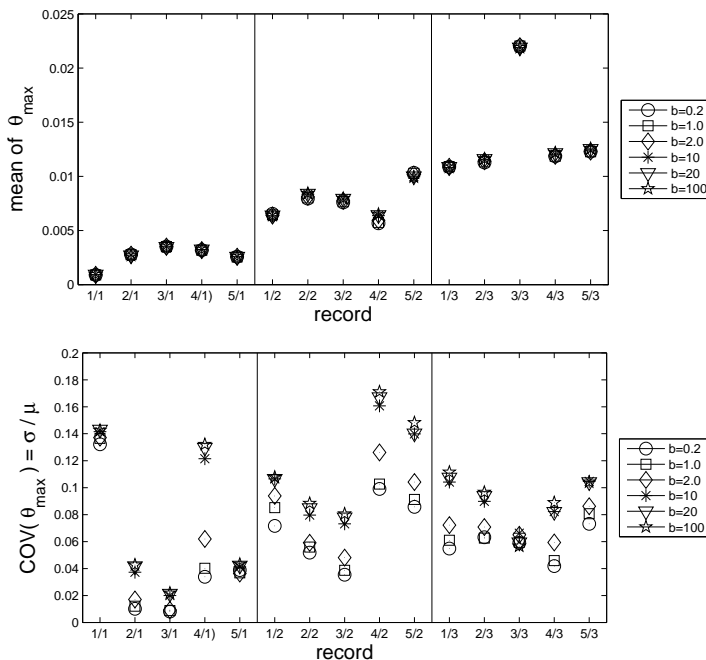
$$COV(\theta_{max}) = \frac{\sigma(\theta_{max})}{E(\theta_{max})}$$

- Investigation of the sensitivity of θ_{max} w.r.t. the correlation length parameter b



A set of sample functions of lognormal stochastic fields characterizing the spatial variation of Young modulus E in a beam

Mean value, COV of θ_{max} for different values of correlation length parameter b and the ground motion records of slide 61 (lognormal distribution of E, σ_y)



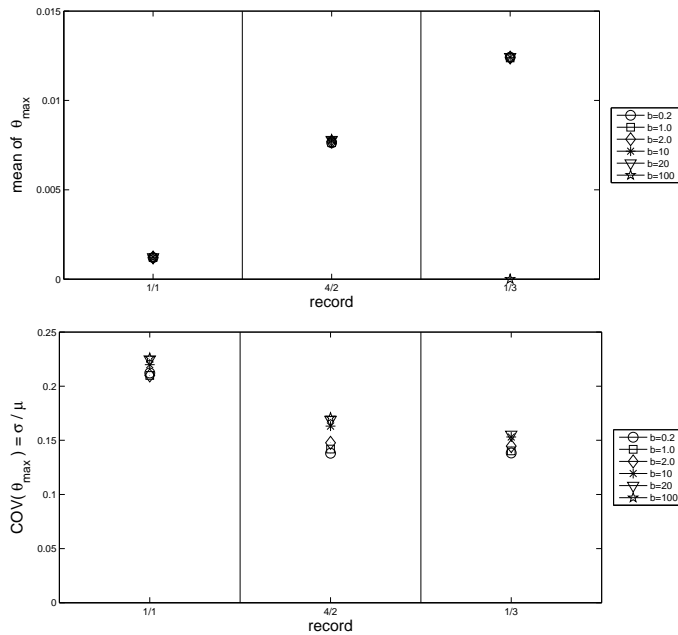
✓ The different characteristics of the seismic records are transferred to the response statistics \implies significant record-to-record variability

✓ The effect of b on COV is important in many cases

✓ A large magnification of uncertainty is observed in some cases \implies max COV=18% ($\sim 1.8\sigma_f$) for record 4/2

✓ The mean value is practically not affected by b

Mean value, COV of θ_{max} for different values of correlation length parameter b and artificial accelerograms compatible with records 1/1, 4/2, 1/3 (lognormal distribution of E, σ_y)



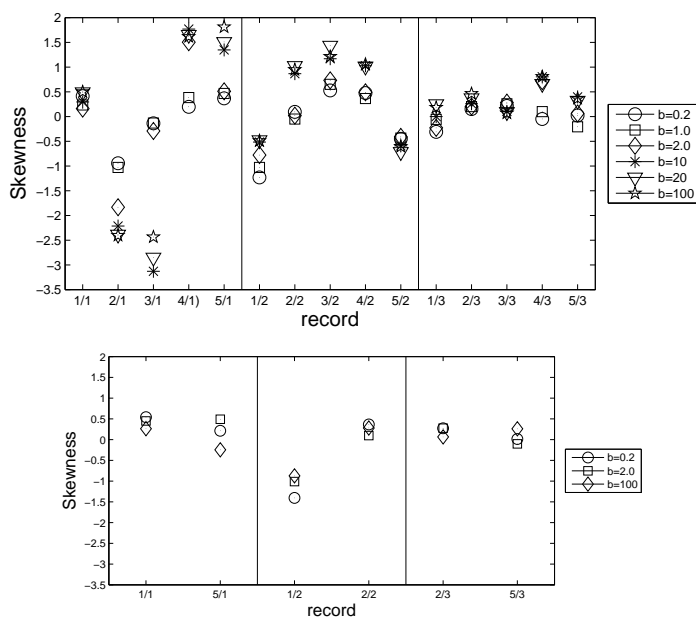
✓ The different characteristics of the seismic records are transferred to the response statistics \implies significant record-to-record variability

✓ The effect of b on COV is important in some cases

✓ The magnification of uncertainty is even more pronounced in this case: max COV=23% ($\sim 2.3\sigma_\theta$) for record 1/1

✓ The mean value is practically not affected by b

Skewness of θ_{max} for different values of correlation length parameter b and the ground motion records of slide 61 (lognormal, L-beta distribution of E, σ_y)



Input skewness values:
 - Lognormal distribution: 0.3
 - L-beta distribution: 0.59

✓ Important record-to-record variability
 ✓ Significant influence of b in many cases

✓ Values of skewness substantially different from those of the system properties due to the strong non-linearity of the problem

• Conclusions

- ✓ A stochastic response history analysis of a steel frame having uncertain non-Gaussian material properties and subjected to seismic loading has been performed.
- ✓ The Young modulus and the yield stress were described by uncorrelated homogeneous non-Gaussian translation fields.
- ✓ The effect of the probability distribution of the input parameters on the response variability was negligible due to the small input COV(=10%).
- ✓ The significant influence of the scale of correlation of the stochastic fields and of the different seismic records on the response variability has been revealed.
- ✓ A large magnification of uncertainty has been observed in some cases.
- ✓ Importance of a realistic uncertainty quantification and propagation in nonlinear dynamic analysis of engineering systems.

Thank you for your attention!